Emergent Materials (2023) 6:1577–1587
https://doi.org/10.1007/s42247-023-00554-4

ORIGINAL ARTICLE

Revealing the in vitro cytotoxicity potential of chitosan-mediated SiO_2/ZnO nanocomposites on the human MCF-7 cell line

Jenson Samraj Jeyaprakash[1] · Perachiselvi Murugan[1] · Satheesh Kumar Balu[2] · Gurusamy Annadurai[1]

Received: 25 May 2023 / Accepted: 4 September 2023 / Published online: 12 September 2023

Abstract

In this study, chitosan nanoparticles (CSNP) were composited with silicon dioxide and zinc oxide (SiO_2/ZnO) using the ionic-gelation process and sodium tripolyphosphate (STPP) as a cross-linking agent. The prepared materials were characterized using XRD, SEM, FTIR, and PSA. The average crystalline sizes were calculated as 23, 22, and 83 nm for CSNP, CSNP-SiO_2 NC, and CSNP-SiO_2/ZnO NC, respectively. The morphology of CSNP, CSNP-SiO_2 NC, and CSNP-SiO_2/ZnO NC was observed to be rod, spherical, and prismatic, which can significantly impact on biomedical applications. The FTIR results indicated that SiO_2 and ZnO were well incorporated into chitosan, suggesting that SiO_2 and ZnO nanoparticles were evenly dispersed throughout the chitosan matrix and chemically bonded into the CSNP. The anticancer efficacy of the prepared samples was tested in MCF-7 breast cancer cell lines at concentrations ranging from 7.8 to 1000 (µg/mL). The samples revealed a dose-dependent inhibitory effect with the maximum effect occurring at 1000 µg/mL. Among the three, CSNP-SiO_2/ZnO NC showed the most pronounced anticancer efficacy compared to CSNP and CSNP-SiO_2 NC.

Keywords Breast cancer · CSNP-SiO_2/ZnO · Cytocompatibility · Ionic-gelation · MCF-7 cell line

Highlights
- The findings of the present investigation provide novel methods for the synthesis of CSNPs, CSNP-SiO_2 NC, and CSNP-SiO_2/ZnO nanocomposites.
- Their formation was validated by X-ray diffraction (XRD), scanning electron microscope (SEM), Fourier transform-infrared (FTIR), and particle size analyzer (PSA).
- Anticancer efficacy of all the three CSNPs was tested in MCF-7 breast cancer cell lines, at different concentrations, and a comparison was made.
- Of the three CSNPs, the anticancer efficacy of CSNP-SiO_2/ZnO NC was more pronounced as compared to CSNP-SiO_2 NC and CSNP.
- These findings imply that incorporating SiO_2/ZnO to CSNP enhances the anticancer efficacy and therefore, synthesizing CSNP-SiO_2/ZnO nanocomposites is an effective therapeutic strategy to inhibit cancer cell growth.

✉ Jenson Samraj Jeyaprakash
jensonsamraj@gmail.com

[1] Division of Environmental Science, Sri Paramakalyani Centre of Excellence in Environmental Sciences, Manonmaniam Sundaranar University, Tamil Nadu, Alwarkurichi 627 412, India

[2] Department of Oral Pathology, Saveetha Dental College and Hospitals, Saveetha Institute of Medical and Technical Sciences, Chennai 600077, Tamil Nadu, India

1 Introduction

Cancer continues to be a major public health problem worldwide, with a growing number of cases. It is projected that by 2030, there will be 21 million new cancer cases. In particular, breast cancer is the leading cause of female mortality worldwide [1]. Several modern treatments are available to treat breast cancer, and most therapies have a high recurrence rate [2]. Therefore, the search for effective anticancer agents is increasing worldwide. Generally, chemotherapy is the preferred treatment for most cancer patients due to its universality and excellent efficacy [3]. Unfortunately, the majority of chemotherapy drugs have poor solubility and permeability, which results in low bioavailability and inadequate drug concentration at the site of the tumor which can limit their effectiveness and increase the likelihood of side effects [4].

Chitosan is a naturally derived cationic polymer that comes from chitin which can be found in the cell walls of fungi, the exoskeletons of crustaceans, insects, and fish scales [5]. It is composed of (1–4)-2-amino-2-deoxy-β-D -glucan. Chitosan has gained attention due to its pH sensitivity, biocompatibility, and bioactive functions. These properties make it more attractive as a potential drug

delivery system compared to its base polymer, chitin [6]. In addition to its other properties, chitosan has also been found to open the tight junctions between epithelial cells, which increases the permeability of the carried drugs [7]. This feature enhances the efficiency of the drug delivery system and the ability of the drugs to reach the targeted cancer cells. Among polymeric nanoparticles, chitosan-based nanoparticles (CSNP) have been extensively investigated as efficient drug delivery biopolymers due to their intriguing biodegradability and biocompatibility properties [8]. CSNP is efficient, cost-effective, chemically inert, non-toxic, and environmentally friendly [9, 10]. It is also utilized as a potential drug delivery system due to their cationic properties, ability to form electrostatic interactions, and biodegradability [11]. These properties make it a versatile and effective system for targeted drug delivery to cancer cells. Because of their small size, CSNP is easily internalized by cells, which enables them to deliver drugs more precisely [12]. These nanoparticles can enhance the accumulation of drugs in cancer cells by increasing permeability and retention [13]. Therefore, CSNP formulations have the potential to revolutionize cancer diagnosis and treatment by providing a more precise and effective way to deliver drugs to cancer cells while minimizing harm to healthy cells. Moreover, the potential applications of CSNP are vast and include ongoing research to identify the signaling pathways that are altered by Ch-Np in cancer cells, which would help in developing more specific and effective cancer therapies [14]. Karthikeyan et al. (2020) synthesized CSNP-loaded curcumin as a natural anticancer agent and evaluated its anticancer activity against MCF-7 cell lines. The results showed that the CSNP-curcumin conjugates displayed higher cytotoxicity against cancer cells compared to bare curcumin. The authors concluded that CSNP can effectively enhance the anticancer activity of curcumin in MCF-7 cell lines (Karthikeyan et al., 2020). In another study, Gonzalez et al. (2015) investigated the anticancer and antimicrobial properties of ZnO nanoparticles with different morphologies (spherical, hexagonal, and rod-like). They found that the different shapes of the nanoparticles affected their biological activity in which the rod-shaped nanoparticles had the most potent anticancer and antimicrobial properties (Gonzalez et al., 2015). Similarly, Gupta et al. [15] investigated the anticancer activity of CSNP loaded with paclitaxel and evaluated its activity against MCF-7 cell lines. These results showed that the CSNP-paclitaxel conjugates displayed a significant inhibitory effect on the proliferation of cancer cells and induced apoptosis. The authors concluded that CSNP can be used as an effective drug delivery system for paclitaxel in the breast cancer treatment [15]. In addition, several studies have also reported the use of CSNP for targeted delivery of anticancer drugs, such as doxorubicin, to MCF-7 cell lines. These studies have shown that the targeted delivery of drugs by CSNP can increase the efficacy of the treatment while reducing side effects. When CSNPs are combined with SiO_2 and ZnO, they can form a composite nanomaterial that exhibits enhanced properties and functionality. SiO_2, also known as silica, is a widely used material due to its excellent biocompatibility, low toxicity, and high stability (Chenicheri et al., 2018). ZnO is a well-known semiconductor material that has been extensively used in various applications due to its unique optical, electronic, and antibacterial properties (Rajeshkumar et al., 2019). The combination of CSNPs with SiO_2 and ZnO can lead to the development of a new composite nanomaterial that exhibits enhanced antibacterial, antioxidant, and biocompatibility properties, as compared to other metal-based nanoparticles. Moreover, the synergistic effects of the three materials can lead to enhanced efficiency in various applications, such as anticancer, drug delivery, wound healing, and water treatment. The advantages of this nanocomposite over the other metals are listed in Table 1.

Therefore, the current study is aimed at developing an NC with effective anti-cancer properties against breast cancer cells. To achieve this, we used a simple ionic gelation method to design three different nanocomposites: CSNP, CSNP-SiO_2 NC, and CSNP-SiO_2/ZnO NC. To ensure that the prepared nanocomposites met the necessary specifications, several analytical techniques were employed to characterize them. X-ray diffraction (XRD) was used to examine their crystal structures, while SEM was used to examine their morphology. Fourier transform-infrared spectroscopy (FTIR) was used to identify their chemical compositions, and particle size analyzer (PSA) was used to measure their particle sizes. Finally, the anticancer activity of the prepared nanocomposites was evaluated using the MTT assay to test the efficacy of the nanocomposites against cancer cells.

2 Materials and methods

2.1 Chemicals and reagents

Biowaste crab shells were collected from the local fish market in Tirunelveli, India, as a chitosan source. Analytical grade chemicals such as SiO_2, ZnO, STPP, sodium hydroxide (NaOH), potassium permanganate ($KMNO_4$), oxalic acid ($C_2H_2O_4$), acetic acid (CH_3 COOH), and hydrochloric acid (HCl) were purchased from Merck (Darmstadt, Germany). Dulbecco's modified Eagle's medium (DMEM), fetal bovine serum (FBS), and phosphate-buffered saline (PBS) were from Gibco, Invitrogen Life Technologies. Additionally, trypsin, ethylenediaminetetraacetic acid, sodium bicarbonate, 3-(4,5-dimethylthiazol-2-yl)-2,5-diphenyltetrazolium bromide (MTT), dimethyl sulfoxide (DMSO), penicillin,

Table 1 Performance comparison of various materials with high potential toxicity towards human MCF-7 cells

Catalyst	Concentration (µg/mL)	Cell line	Morphology	Cytotoxicity effect (%)	Reference
CSNP-SiO_2/ZnO NC	1000	MCF-7	Prismatic	85	Present work
Au	48	MCF-7	-	67	[36]
ZnO	10	MCF-7	Nanorod	60	[37]
ZrO	500	MCF-7	Nanoclusters	18	[24]
Ag NPs	60	MCF-7	Spherical	56	(Khorrami et al., 2018)
$NiFe_2O_4$ NPs	500	MCF-7	Spherical	24.92	(Sarala et al., 2022)

and streptomycin were obtained from Sigma-Aldrich for the experiments.

2.2 Chitosan preparation from crab shells

The process of extracting chitosan from crab shells involved the following steps: first, the shells were washed with running tap water and then cleaned with acetone and ethanol to remove any impurities. After that, the shells were exposed to sunlight for 24 h to dry. Then, the shells underwent a series of chemical procedures such as demineralization, deproteinization, deacetylation, and decoloration to extract chitosan. As part of the demineralization process, the ground shells were treated with 5% hydrochloric acid for 6 h at room temperature. This process helps to remove any inorganic materials from the crab shells and is crucial in the extraction of chitosan. The filtered solid materials were collected, dried, and then washed with deionized water until they reached a pH of 7. The solid materials were then treated with a 5% NaOH solution, and the contents were stirred for 6 h at 80 °C with a solid-to-solvent ratio of 1:10 (w/v). The residue was then washed, filtered, and dried for 12 h at room temperature. The next step was deacetylation, which was carried out by treating the solid materials with 45% NaOH at 120 °C for 24–48 h with a solid-to-solvent ratio of 1:10 (w/v). The final step was decoloration, which was done by treating the resulting chitosan with 1% $KMnO_4$ and 1% oxalic acid $(COOH)_2$ for 1 h. The obtained chitosan was then used to prepare the CSNP [16].

2.3 Preparation of chitosan nanoparticles

The CSNP was prepared using the ionic gelation technique. The process involved dissolving the obtained chitosan powder in a 1% acetic acid aqueous solution and stirring it continuously at room temperature for 24 h until a clear solution was obtained. Then, a 0.1% STPP solution was added dropwise to the chitosan solution. The resulting mixture was kept under constant stirring in the room temperature for 12 h and subsequently dried in a hot air oven at 60 °C for 12 h to obtain CSNP.

To synthesize the CSNP-SiO_2 nanocomposite, 1:1 ratio of CSNP and SiO_2 was mixed with 100 mL of distilled water, and the mixture was continuously stirred. The reaction was maintained for 4 h. Afterward, the nanocomposite was centrifuged multiple times using distilled water and ethanol and then dried in a hot air oven at 80 °C. Subsequently, the CSNP-SiO_2 nanocomposite was calcined at 800 °C for 3 h. The same procedure was adopted for the synthesis of the CSNP-SiO_2/ZnO nanocomposite. The step-by-step preparation of the synthesized CSNP-SiO_2/ZnO nanoparticles is illustrated in Fig. 1.

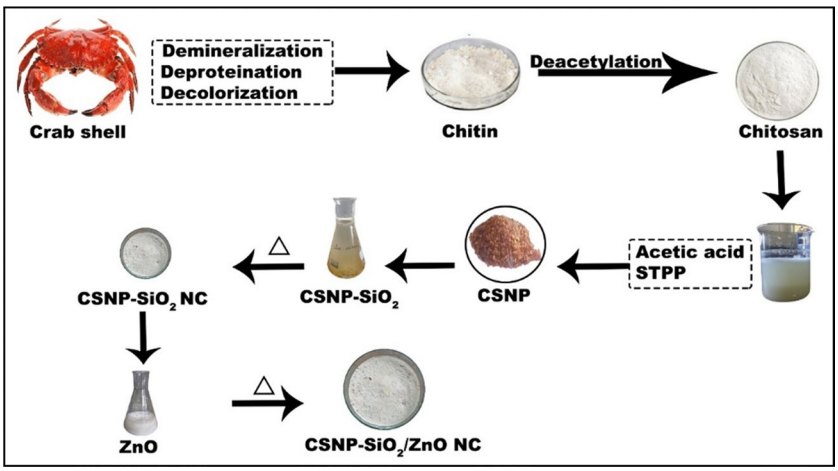

Fig. 1 Schematic depiction of synthesized CSNP, CSNP-SiO_2, and CSNP-SiO_2/ZnO NC

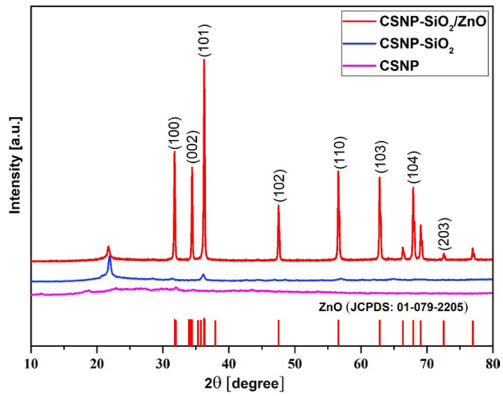

Fig. 2 XRD patterns of CSNP, CSNP-SiO_2, and CSNP-SiO_2/ZnO NC

2.4 Characterization of CSNP and NC

To analyze the formation of nanoparticles, a UV-spectrophotometer (Implen GmBH) was used to scan the solution in the range of 200–600 nm. The scan was done using a quartz cuvette with water as the reference. The crystalline structure of prepared CSNP, CSNP-SiO_2 NC, and CSNP-ZnO NC was investigated using X-ray diffraction (XPERT- PRO diffractometer). The size and morphology of the nanoparticles were examined by SEM on CAREL ZEISS (Model: EVO 18). To examine the samples using SEM, a small amount of vacuum-dried CSNP was placed on a stub using double-sided adhesive tape and then coated with a thin layer of metal using a sputtering process at 50 mA for 6 min. After that, the stub was inserted into the SEM chamber and a photomicrograph was taken at an acceleration voltage of 20 kV. A particle size analysis was performed on Micromeritics (Model: Nano Plus) to determine the particle size of prepared nanomaterials. FTIR was performed on Perkin Elmer (Model: Spectrum Two) with a range of 4000 to 400 cm^{-1}. The infrared spectra were taken by using a Fourier-transform infrared spectrophotometer

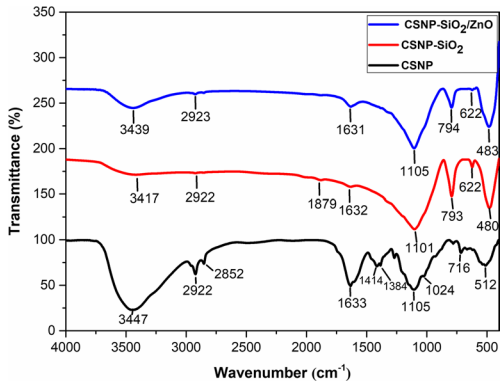

Fig. 3 FTIR spectra of the synthesized CSNP, CSNP-SiO_2 NC, and CSNP-SiO_2/ZnO NC

(FTIR) in the middle infrared range, from 4000 to 400 cm^{-1}, with a resolution of 4 cm^{-1}, in absorbance mode, at room temperature, and with 10 scans. To obtain the FTIR spectra of CSNP, 1 mg of the sample was placed on the sensor of the instrument, and the obtained spectrum was compared with the spectrum of pure chitosan and the TPP standard. This method allows for the identification of the chemical functional groups present in the CSNP and can be used to confirm the presence of chitosan and TPP in the sample.

2.5 Cell line and culture

The MCF-7 breast cancer cell line was obtained from the National Centre for Cell Sciences (NCCS) in Pune, India. The cells were grown in a medium containing Dulbecco's modified Eagle's medium (DMEM) supplemented with 10% fetal bovine serum (FBS), 50 U/mL of penicillin, and 50 µg/mL of streptomycin, under a humidified atmosphere containing 95% air and 5% CO_2, at 37 °C. When the cells reached around 90% confluency, they were detached by adding 2 mL of a solution containing 0.05% trypsin and 0.54 mM EDTA. The cells were then washed thoroughly with media and subcultured in a 75-cm^2 culture flask for expansion. They were then detached again using trypsin at 80% confluency.

2.6 MTT assay

The cell viability was determined using a colorimetric assay called the 3-(4,5-dimethylthiazol-2-yl)-2,5-diphenyl tetrazolium (MTT) assay [17]. Once the cells reached 80% confluency, they were detached using trypsin and then plated with a density of 2×10^5 cells/well in a 24-well microtiter plate. The cells were allowed to adhere for 24 h in a CO_2 incubator. The cells were then treated with different concentrations of CSNP, CSNP-SiO2 NC, and CSNP-SiO_2/ZnO NC in quadruplicate. After 24 h of incubation, 10 µl of MTT dye (5 mg/mL in PBS) was added to each well and incubated for 4 h in a 5% CO_2 incubator. This allowed the active live cells to convert the water-soluble yellow MTT solution into a water-insoluble purple formazan. After incubation, the purple-colored formazan crystals trapped in cells were solubilized in 150 µL of DMSO and the optical density was measured in each well, including the blanks at 560 nm using a microplate reader. The cell viability was determined using the formula mentioned below.

$$\text{Cell Viability (\%)} = (\text{A\_570 of treated cells})/(\text{A\_570 of control cells}) \times 100$$

3 Results and discussion

3.1 X-ray diffraction (XRD)

An XRD analysis was performed on CSNP, CSNP-SiO_2 NC, and CSNP-SiO_2/ZnO NC to examine the crystallinity.

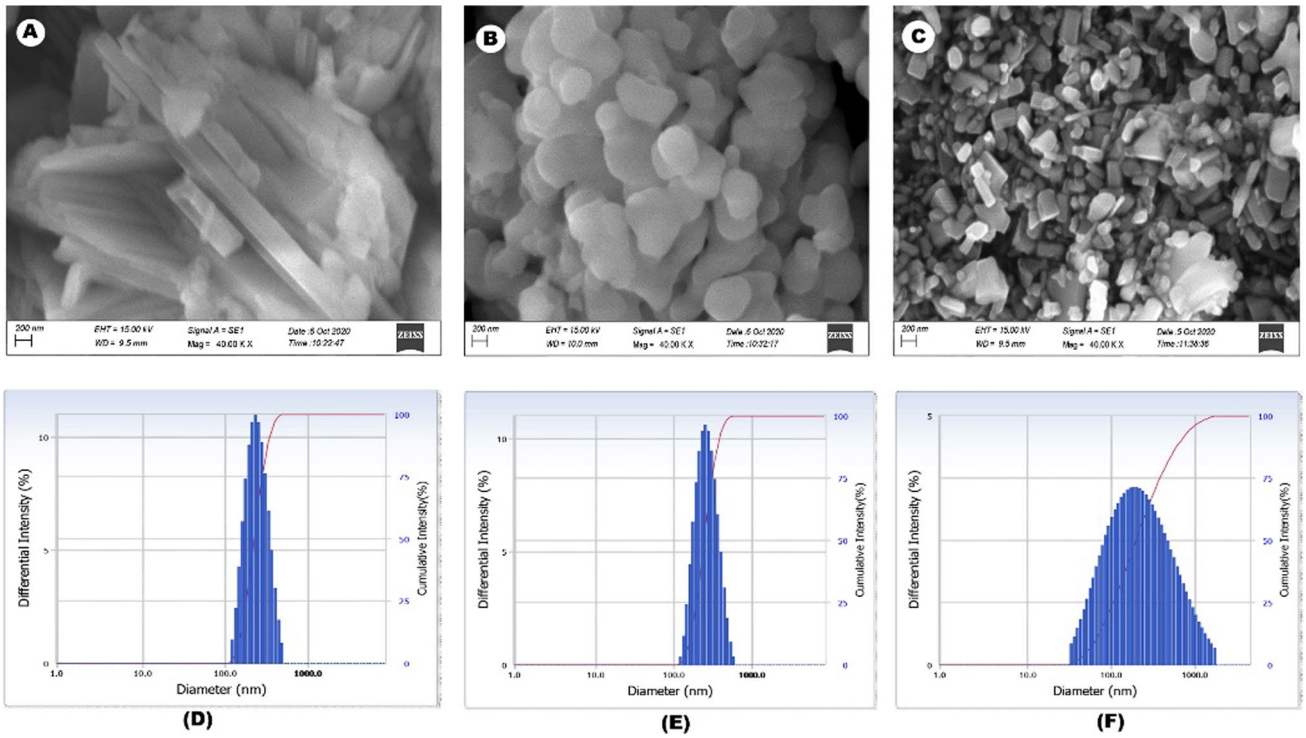

Fig. 4 SEM image of **A** CSNP, **B** CSNP-SiO_2 NC, and **C** CSNP-SiO_2/ZnO NC and the particle size distribution of **D** CSNP, **E** CSNP-SiO_2 NC, and **F** CSNP-SiO_2/ZnO NC

Figure 2 shows the XRD patterns of prepared materials, and the peaks observed at 22.82° and 37.52° indicate the presence of SiO_2 in the NC. The diffraction peaks recorded at 31.76°, 34.41°, 36.25°, 47.53°, 56.59°, 62.85°, 81.37°, and 89.60° correspond to (100), (002), (101), (102), (110), (103), (104), and (203) planes of ZnO, respectively (JCPDS card no: 01–079-2205) [18]. The average crystalline size of CSNP, CSNP-SiO_2 NC, and CSNP-SiO_2/ZnO NC was calculated using the following Scherer formula and was found to be 23, 22, and 83 nm.

$$D = K\lambda/\beta\cos\theta$$

where the crystallite size, D, to the full width at half maximum (FWHM) of the peak at half of the maximum intensity, β, the diffraction wavelength, λ, the diffraction angle, θ, and a constant K that is related to the crystallite shape and is approximately 0.94.

3.1.1 FTIR

The functional groups of CSNP, CSNP-SiO_2 NC, and CSNP-SiO_2/ZnO NC were analyzed, and the results are shown in Fig. 3. The broad absorption band of CSNP between 3400 and 3450 cm^{-1} is attributed to the stretching vibration of $-NH_2$ and $-OH$ groups. Chitosan is biodegradable, biocompatible, non-toxic, and has a wide range of potential applications due to the presence of OH and NH_2 groups [19]. The peaks between 2800 and 2852 cm^{-1} are attributed to the C–H asymmetric stretching and C–H stretching of CH_2, respectively [20]. The peak registered at 1414 cm^{-1} corresponds to the CH_3 symmetrical deformation mode, and the band at 1384 cm^{-1} corresponds to the C-O stretching of the primary alcoholic group [21, 22]. The peak at 1105 cm^{-1} corresponds to C–O–C stretching, and the peak at 1024 cm^{-1} is attributed to both C–N (primary amines) and C–O (primary alcohol) stretching vibrations in chitosan [23]. The sharp peak at 716 cm^{-1} is because of 1, 2 di-substituted C–Cl stretching [24]. The broad absorption band at 3447 cm^{-1} from CSNP is reduced to a narrow peak when CSNP was incorporated with SiO_2, and the same peak widened when incorporated with SiO_2 and ZnO. The same trend was observed for the peak arising at 1633 cm^{-1}, and a few peaks at 1414, 1384, and 1024 cm^{-1} disappeared after incorporation. The absorption band below 700 cm^{-1} is attributed to SiO_2 and ZnO stretching vibration. These results suggest that the SiO_2 and ZnO were well incorporated into CSNP.

3.1.2 SEM

The SEM images in Fig. 4A–C depict various morphologies of the prepared CSNP, CSNP-SiO_2 NC, and CSNP-SiO_2/

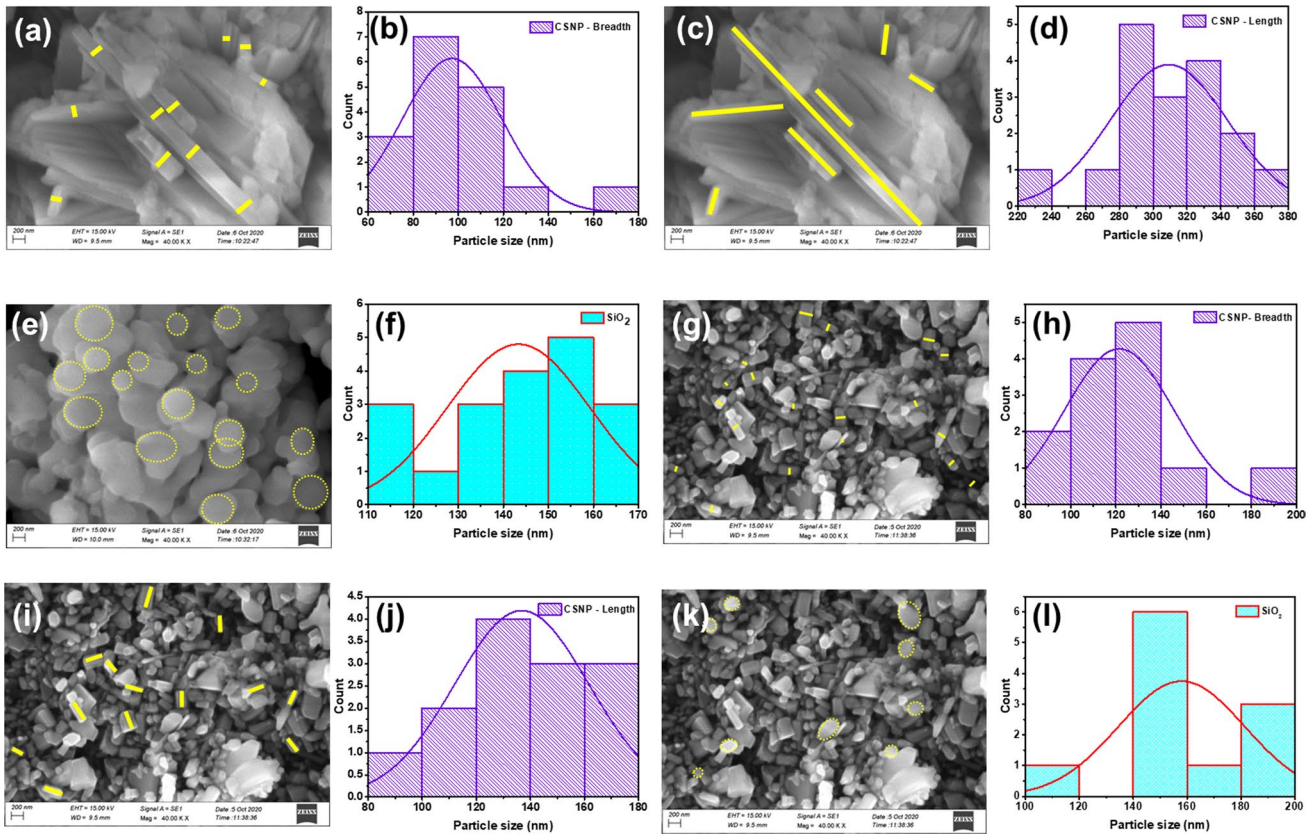

Fig. 5 SEM images of **a**, **c** CSNP, **e** CSNP-SiO_2 NC, and **g**, **i**, **k** CSNP-SiO_2/ZnO NC, along with particle size distributions of **b** CSNP (breadth), **d** CSNP (length), **f** SiO_2 in CSNP-SiO_2 NC, **h** breadth of CSNP in CSNP-SiO_2/ZnO NC, **j** length of CSNP in CSNP-SiO_2/ZnO NC, and **l** SiO_2 in CSNP-SiO_2/ZnO NC

ZnO NC, with smaller aggregations in the form of rods, spherical, and prismatic shapes, respectively. These morphologies make them potential candidates for biomedical applications, as the shape of the materials plays an essential role in their properties. For example, rod-shaped nanomaterials are thought to be well-suited for drug and gene delivery applications as they have the ability to effectively enter cells, as reported in prior studies [25, 26]. Spherical nanomaterials also have potential in drug delivery applications, particularly for sustained release of drugs over a prolonged period of time. Their spherical shape allows them to be easily taken up by cells and can be used for targeted drug delivery to cancer cells through their surface functionalization [27, 28]. Prismatic shapes have the ability to act as scaffolds for cell growth and tissue engineering, due to their large surface area, which can be functionalized to support cell adhesion and proliferation. They can also be used as scaffolds for drug delivery, allowing for the controlled release of drugs over time [29].

As observed in SEM images, the change in particle diameter or size observed in the CSNP-SiO_2 nanocomposite and its decrease upon adding ZnO can be attributed to several underlying mechanisms: in the CSNP-SiO_2 nanocomposite, the SiO_2 shell is formed around the CSNP core, which increases the overall particle size. The thickness of the SiO_2 shell can vary depending on the synthesis conditions and reaction time. Adding ZnO to the nanocomposite may result in a thinner ZnO layer compared to the SiO_2 shell, leading to a decrease in particle size [30]. During the synthesis process,

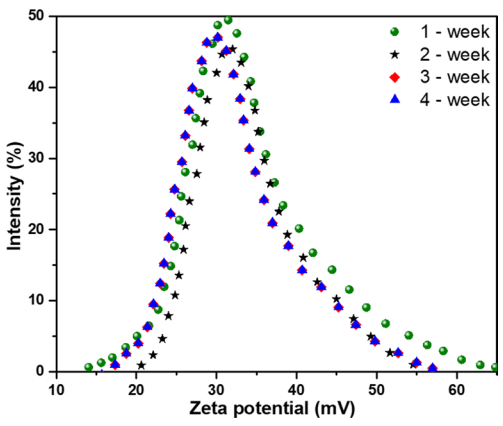

Fig. 6 Effect of time on zeta potential of the as-developed nanoparticle suspensions

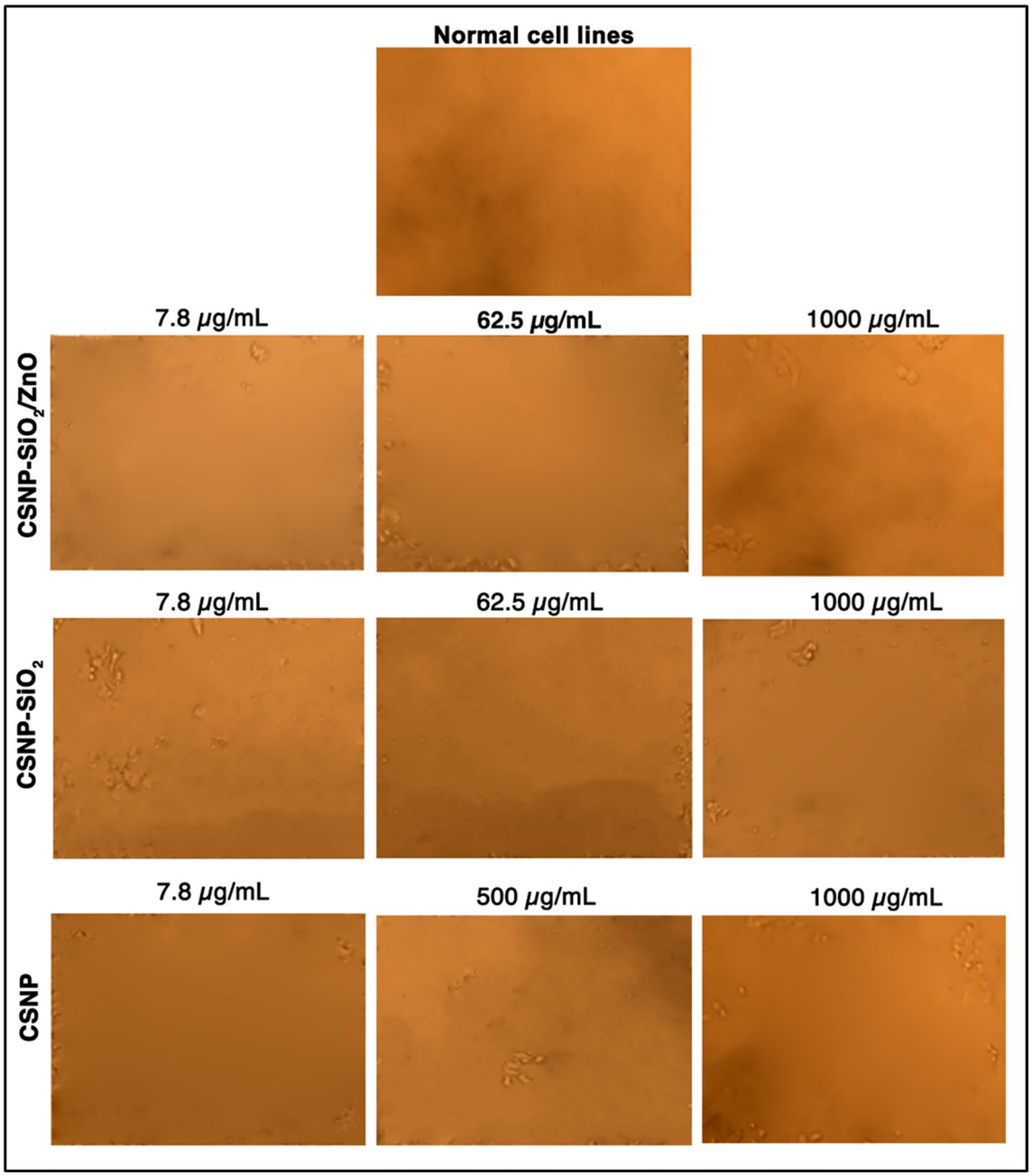

Fig. 7 Anticancer effects of CSNP, CSNP-SiO_2 NC, and CSNP-SiO_2/ZnO NC on normal breast cell line

CSNP-SiO_2 nanocomposite may have a tendency to aggregate or agglomerate due to interparticle interactions, such as van der Waals forces or electrostatic interactions. This aggregation can contribute to an increase in particle size. When ZnO is added, it may help to disrupt the aggregation and promote a more dispersed state, resulting in a decrease in particle size [31]. The addition of ZnO to the CSNP-SiO_2 nanocomposite may induce crystallinity changes or phase transformations in the composite structure. Depending on the specific crystalline phases formed, it could affect the particle size. For example, the formation of ZnO nanoparticles with a different crystal structure may result in smaller particle sizes compared to the CSNP-SiO_2 nanocomposite [32].

3.2 Particle size analyzer (PSA)

The average particle size of the CSNP, CSNP-SiO_2 NC, and CSNP-SiO_2/ZnO NC were determined using PSA and are shown in Fig. 4D–F. The results show that the average

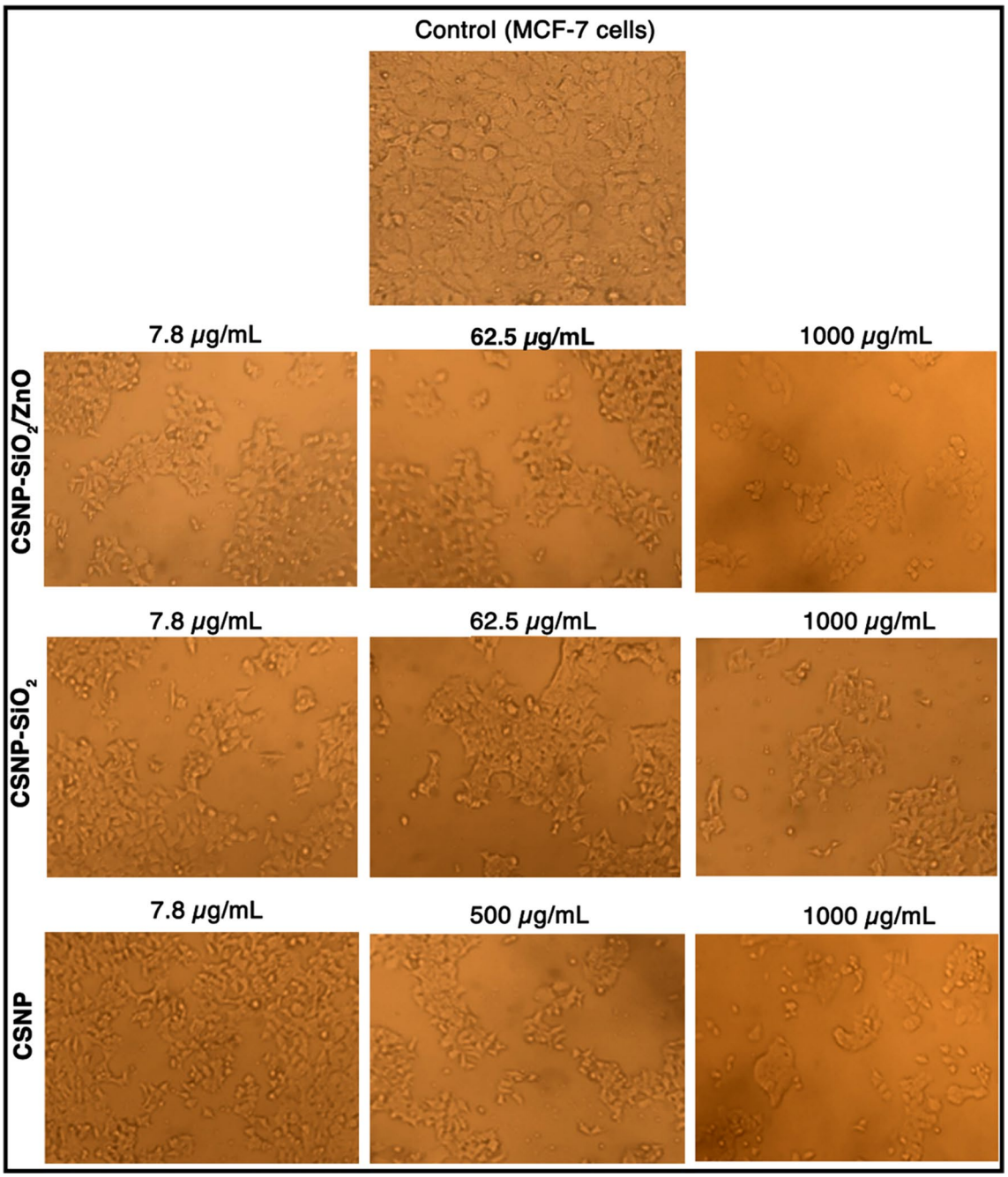

Fig. 8 Anticancer effects of CSNP, CSNP-SiO_2 NC, and CSNP-SiO_2/ZnO NC on MCF-7 cell line

particle size of CSNP, CSNP-SiO_2 NC, and CSNP-SiO_2/ZnO NC were 268.9, 278.7, and 318 nm, respectively. The polydispersity index of CSNP, CSNP-SiO_2 NC, and CSNP-SiO_2/ZnO was 0.550, 0.382, and 0.306, respectively. These results demonstrate that the addition of SiO_2 and ZnO to CSNP leads to an increase in the particle size. The SEM images along with the particle size distribution curve of CSNP, CSNP-SiO_2 NC, and CSNP-SiO_2/ZnO are displayed in Fig. 5.

3.3 Stability of the CSNP-SiO_2/ZnO in different pH conditions

The stability of the CSNP-SiO_2/ZnO nanocomposite suspension was investigated at different pH levels as depicted in Fig. 6 [33]. The pH control plays a crucial role in stability control by determining the suspension's iso-electric point (IEP) to prevent coagulation and instability. The zeta potential value of the as-prepared CSNP-SiO_2/ZnO

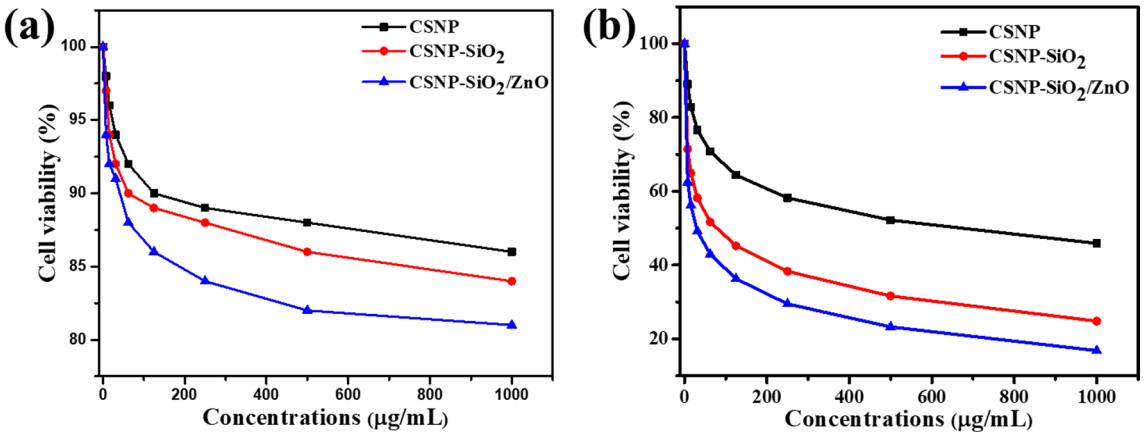

Fig. 9 **a** Dose-dependent growth inhibition of normal breast cells and **b** breast cancer cells (MCF-7 cell line) by CSNP, CSNP-SiO_2, and CSNP-SiO_2/ZnO

NC was 34.2 mV. After 1, 2, 3, and 4 weeks of storage, the zeta potential values of the same suspension were 33.5, 32.3, 30.5, and 30.4 mV, respectively. These values indicate that there is enough electrostatic repulsion force between particles to prevent attraction and collision caused by Brownian motion. However, over time, the zeta potential values gradually decreased, indicating the occurrence of particle agglomeration and aggregation in the suspension. Nevertheless, the zeta potential values demonstrate that the CSNP-SiO_2/ZnO NC suspension remains stable, even after 4 weeks of storage at different pH levels.

3.4 Anticancer activity

The anticancer efficacy of CSNP, CSNP-SiO_2 NC, and CSNP-SiO_2/ZnO NC was tested on both normal breast cells and MCF-7 cell line at different concentrations (7.8, 15.6, 31.2, 62.5, 125, 250, 500, and 1000 µg/mL) as depicted in Fig. 7. The corresponding graph is displayed in Fig. 9a. The CSNP-SiO_2/ZnO NC exhibited lower cell toxicity towards the normal breast cells compared to CSNP and CSNP-SiO_2 NC, respectively. This can be attributed to the formation of a unique structure or surface properties that minimize interactions with normal breast cells, thus reducing their toxicity. From Fig. 9a, it is evident that CSNP-SiO_2/ZnO NC exhibited dose-dependent relationship with CSNP and CSNP-SiO_2 NC, reducing cell viability by 14% compared to CSNP and CSNP-SiO_2 NC at 1000 µg/mL.

In contrast, for breast cancer cells, the results showed that CSNP-SiO_2/ZnO NC exhibited 85% anticancer activity than CSNP (54%) and CSNP-SiO_2 NC (68%) at 1000 µg/mL (Figs. 8 and 9b). These results align with previous research, which has shown that doped and hybrid nanoparticles have improved anticancer activity and biocompatibility compared to pure nanoparticles. For instance, [34, 35] found that SnO_2-doped ZnO/reduced graphene nanoparticles (NCs) had superior anticancer activity and biocompatibility in comparison to SnO_2-ZnO nanoparticles and ZnO nanoparticles. Furthermore, our study revealed that the cytotoxic effect of CSNP-SiO_2/ZnO NC was as high as 85%, which is a greater result than those previously reported by Elsayed et al. [36] and Kavithaa et al. [37]. The outcome from the value of 85% cytotoxic effect of CSNP-SiO_2/ZnO NC suggests that this nanoparticle has strong potential as an anticancer agent. It indicates that at 1000 µg/mL concentration, the nanocomposites were able to kill 85% of the cancer cells in the MCF-7 cell line. Additionally, the nanocomposite high surface area may also contribute to its cytotoxicity by promoting cellular uptake and disrupting cellular processes [38]. Furthermore, chitosan-mediated SiO_2/ZnO nanocomposites may induce apoptosis (programmed cell death) in cancer cells by activating various signaling pathways involved in apoptosis, such as the caspase cascade, the p53 pathway, and the mitochondrial pathway. Also, it has been proposed that chitosan-mediated SiO_2/ZnO nanocomposites may also exert their anticancer activity by inhibiting the growth and proliferation of cancer cells by disrupting the cell cycle, altering gene expression, and inducing oxidative stress [39].

4 Conclusion

In this study, CSNP were produced using the ionic-gelation technique and then combined with SiO_2 and ZnO to create CSNP-SiO_2 NC and CSNP-SiO_2/ZnO NC respectively. The properties of all three types of NCs were analyzed using XRD, SEM, FTIR, and PSA methods. The XRD analysis showed that the average crystalline sizes of CSNP, CSNP-SiO_2 NC, and

CSNP-SiO_2/ZnO NC were 23 nm, 22 nm, and 83 nm, respectively. The SEM images revealed that the morphology of CSNP, CSNP-SiO_2 NC, and CSNP-SiO_2/ZnO NC were rod, spherical, and prismatic respectively. The anticancer efficacy of all three types of CSNP was evaluated on the MCF-7 breast cancer cell line at different concentrations (7.8 to 1000 µg/mL). All three types of CSNP showed a dose-dependent inhibitory effect, with the highest effect observed at 1000 µg/mL. CSNP-SiO_2/ZnO NC was found to have more cytotoxicity than CSNP-SiO2 NC and CSNP. These results indicate that incorporating SiO_2/ZnO NC into CSNP improves their anticancer efficacy. Therefore, the synthesis of CSNP-SiO_2/ZnO NC is an effective strategy for inhibiting cancer cell growth.

Acknowledgements The authors would like to express our gratitude to Dr. Manju and Dr. Samuel Rajendran for their guidance and support throughout the course of this study.

Author contribution Jenson Samraj Jeyaprakash: conceptualization, methodology, validation, investigation, data curation, and writing—original draft. Murugan Perachiselvi: validation and investigation. Satheesh Kumar Balu: validation and investigation. Annadurai Gurusamy: resources, supervision, and writing—review and editing.

Data availability The data will be made available on reasonable request from the corresponding author.

Declarations

Conflict of interest The authors declare no competing interests.

References

1. F. Bray, J. Ferlay, I. Soerjomataram, R.L. Siegel, L.A. Torre, A. Jemal, Global cancer statistics 2018: GLOBOCAN estimates of incidence and mortality worldwide for 36 cancers in 185 countries. CA. Cancer J. Clin. **68**(6), 394–424 (2018). https://doi.org/10.3322/caac.21492
2. A.M. Gonzalez-Angulo, F. Morales-Vasquez, G.N Hortobagyi, Overview of resistance to systemic therapy in patients with breast cancer. *Advances in Experimental Medicine and Biology*, 1–22 (2007). https://doi.org/10.1007/978-0-387-74039-3_1
3. S.-E. Al-Batran, N. Homann, C. Pauligk, T.O. Goetze, J. Meiler, S. Kasper, H.-G. Kopp, F. Mayer, G.M. Haag, K. Luley, U. Lindig, W. Schmiegel, M. Pohl, J. Stoehlmacher, G. Folprecht, S. Probst, N. Prasnikar, W. Fischbach, R. Mahlberg, J. Trojan, Perioperative chemotherapy with fluorouracil plus leucovorin, oxaliplatin, and docetaxel versus fluorouracil or capecitabine plus cisplatin and epirubicin for locally advanced, resectable gastric or gastro-oesophageal junction adenocarcinoma (FLOT4): a randomised, phase 2/3 trial. The Lancet **393**(10184), 1948–1957 (2019). https://doi.org/10.1016/s0140-6736(18)32557-1
4. X. Jia, Y. Zhang, Y. Zou, Y. Wang, D. Niu, Q. He, Z. Huang, W. Zhu, H. Tian, J. Shi, Y. Li, Cancer therapy: dual intratumoral redox/enzyme-responsive NO-releasing nanomedicine for the specific, high-efficacy, and low-toxic cancer therapy. Adv. Mater. **30**(30), 1870217 (2018). https://doi.org/10.1002/adma.201870217
5. L. Qian, K. Zhang, X. Guo, M. Yu, What happens when chitin becomes chitosan? Single-Mol. Stud. RSC Adv. **13**(4), 2294–2300 (2023). https://doi.org/10.1039/d2ra07303j
6. R.N. Wijesena, N. Tissera, Y.Y. Kannangara, Y. Lin, G.A.J. Amaratunga, K.M.N. de Silva, A method for top down preparation of chitosan nanoparticles and nanofibers. Carbohyd. Polym. **117**, 731–738 (2015). https://doi.org/10.1016/j.carbpol.2014.10.055
7. T.-H. Yeh, L.-W. Hsu, M.T. Tseng, P.-L. Lee, K. Sonjae, Y.-C. Ho, H.-W. Sung, Mechanism and consequence of chitosan-mediated reversible epithelial tight junction opening. Biomaterials **32**(26), 6164–6173 (2011). https://doi.org/10.1016/j.biomaterials.2011.03.056
8. W. Fan, B. Yung, P. Huang, X. Chen, Nanotechnology for multimodal synergistic cancer therapy. Chem. Rev. **117**(22), 13566–13638 (2017). https://doi.org/10.1021/acs.chemrev.7b00258
9. A.M. Mandil, T.J. Marjic, B.M. Al-Taanid, A.H. Khalede, .A. Badwan, Depolymerization of HMW into a predicted LMW chitosan and determination of the degree of deacetylation to guarantee its quality for research use. (2018)
10. R. Shanmuganathan, T.N.J.I. Edison, F. LewisOscar, P. Kumar, S. Shanmugam, A. Pugazhendhi, Chitosan nanopolymers: an overview of drug delivery against cancer. Int. J. Biol. Macromol. **130**, 727–736 (2019). https://doi.org/10.1016/j.ijbiomac.2019.02.060
11. A.C. Jayasuriya, Production of micro- and nanoscale chitosan particles for biomedical applications. Chitosan Based Biomater. **1**, 185–209 (2017). https://doi.org/10.1016/b978-0-08-100230-8.00008-x
12. Y. Herdiana, N. Wathoni, S. Shamsuddin, M. Muchtaridi, Drug release study of the chitosan-based nanoparticles. Heliyon. **8**(1), e08674 (2022). https://doi.org/10.1016/j.heliyon.2021.e08674
13. P.Y. Liyanage, S.D. Hettiarachchi, Y. Zhou, A. Ouhtit, E.S. Seven, C.Y. Oztan, E. Celik, Leblanc RM (2019) Nanoparticle-mediated targeted drug delivery for breast cancer treatment. Biochimica et Biophysica Acta (BBA) – Rev. Cancer **2**, 419–433 (1871). https://doi.org/10.1016/j.bbcan.2019.04.006
14. Y. Lv, Y. Lv, Z. Wang, K. Yuan, Y. Zeng, Noncoding RNAs as sensors of tumor microenvironmental stress. J. Exp. Clin. Cancer Res. **41**(1) (2022). https://doi.org/10.1186/s13046-022-02433-y
15. U. Gupta, S. Sharma, I. Khan, A. Gothwal, A.K. Sharma, Y. Singh, M.K. Chourasia, V. Kumar, Enhanced apoptotic and anticancer potential of paclitaxel loaded biodegradable nanoparticles based on chitosan. Int. J. Biol. Macromol. **98**, 810–819 (2017). https://doi.org/10.1016/j.ijbiomac.2017.02.030
16. T.V. Nguyen, T.T.H. Nguyen, S.-L. Wang, T.P.K. Vo, A.D. Nguyen, Preparation of chitosan nanoparticles by TPP ionic gelation combined with spray drying, and the antibacterial activity of chitosan nanoparticles and a chitosan nanoparticle–amoxicillin complex. Res. Chem. Intermed. **43**(6), 3527–3537 (2016). https://doi.org/10.1007/s11164-016-2428-8
17. T. Mosmann, Rapid colorimetric assay for cellular growth and survival: application to proliferation and cytotoxicity assays. J. Immunol. Methods **65**(1–2), 55–63 (1983). https://doi.org/10.1016/0022-1759(83)90303-4
18. M.S. Sivakami, T. Gomathi, J. Venkatesan, H.-S. Jeong, S.-K. Kim, P.N. Sudha, Preparation and characterization of nano chitosan for treatment wastewaters. Int. J. Biol. Macromol. **57**, 204–212 (2013). https://doi.org/10.1016/j.ijbiomac.2013.03.005
19. J. Sukprasert, K. Thumanu, I. Phung-on, C. Jirarungsatean, L.E. Erickson, P. Tuitemwong, K. Tuitemwong, Synchrotron FTIR light reveals signal changes of biofunctionalized magnetic nanoparticle attachment on Salmonella sp. J. Nanomater. **2020**, 1–12 (2020). https://doi.org/10.1155/2020/6149713
20. A. Mahmoud, O. Osman, K. Eid, E. Al Ashkar, A. Okasha, D. Atta, M. Eid, Z. Aziz, A. Fakhry, FTIR spectroscopy of natural biopolymers blends. Middle East J. Appl. Sci. **4**(4), 816–824 (2014)
21. N. Jothi, R. Kunthavai Nachiyar, Identification and isolation of chitin and chitosan from cuttle bone of Sepia prashadi Winckworth, 1936. Global J. Biotechnol. Biochem. **8**(2), 33–39 (2013). https://doi.org/10.5829/idosi.gjbb.2013.8.2.1107
22. M.E. Sotelo-Boyás, Z.N. Correa-Pacheco, S. Bautista-Baños, M.L. Corona-Rangel, Physicochemical characterization of chitosan

nanoparticles and nanocapsules incorporated with lime essential oil and their antibacterial activity against food-borne pathogens. LWT **77**, 15–20 (2017). https://doi.org/10.1016/j.lwt.2016.11.022
23. S. Jana, A. Saha, A.K. Nayak, K.K. Sen, S.K. Basu, Aceclofenac-loaded chitosan-tamarind seed polysaccharide interpenetrating polymeric network microparticles. Colloids Surf., B **105**, 303–309 (2013). https://doi.org/10.1016/j.colsurfb.2013.01.013
24. V. Sai Saraswathi, K. Santhakumar, Photocatalytic activity against azo dye and cytotoxicity on MCF-7 cell lines of zirconium oxide nanoparticle mediated using leaves of Lagerstroemia speciosa. J. Photochem. Photobiol., B **169**, 47–55 (2017). https://doi.org/10.1016/j.jphotobiol.2017.02.023
25. H. Hassan, A. Salama, A.K. El-ziaty, M. El-Sakhawy, New chitosan/silica/zinc oxide nanocomposite as adsorbent for dye removal. Int. J. Biol. Macromol. **131**, 520–526 (2019). https://doi.org/10.1016/j.ijbiomac.2019.03.087
26. C. Lustriane, F.M. Dwivany, V. Suendo, M. Reza, Effect of chitosan and chitosan-nanoparticles on post harvest quality of banana fruits. J. Plant Biotechnol. **45**(1), 36–44 (2018). https://doi.org/10.5010/jpb.2018.45.1.036
27. M.J. Mitchell, M.M. Billingsley, R.M. Haley, M.E. Wechsler, N.A. Peppas, R. Langer, Engineering precision nanoparticles for drug delivery. Nat. Rev. Drug Dis. **20**, 1–24 (2020). https://doi.org/10.1038/s41573-020-0090-8
28. J.K. Patra, G. Das, L.F. Fraceto, E.V.R. Campos, M. Rodriguez-Torres, P. Del, L.S. Acosta-Torres, L.A. Diaz-Torres, R. Grillo, M.K. Swamy, S. Sharma, S. Habtemariam,H.S. Shin, Nano based drug delivery systems: recent developments and future prospects. J. Nanobiotechnol. **16**(1) (2018). https://doi.org/10.1186/s12951-018-0392-8
29. Q.L. Loh, C. Choong, Three-dimensional scaffolds for tissue engineering applications: role of porosity and pore size. Tissue Eng. Part B Rev. **19**(6), 485–502 (2013). https://doi.org/10.1089/ten.teb.2012.0437
30. N. Barth, C. Schilde, A. Kwade, Influence of particle size distribution on micromechanical properties of thin nanoparticulate coatings. Phys. Procedia **40**, 9–18 (2013). https://doi.org/10.1016/j.phpro.2012.12.002
31. A, Singer, Z. Barakat, S. Mohapatra, S.S. Mohapatra, (2019) Nanoscale drug-delivery systems. In Nanocarriers for Drug Delivery (pp. 395–419). Elsevier. https://doi.org/10.1016/B978-0-12-814033-8.00013-8
32. G. Panomsuwan, H. Manuspiya, Correlation between size and phase structure of crystalline BaTiO 3 particles synthesized by sol-gel method. Mater. Res. Express **6**(6), 065062 (2019). https://doi.org/10.1088/2053-1591/ab101b
33. I. Nurdin, S. Ridwan, The effect of pH and time on the stability of superparamagnetic maghemite nanoparticle suspensions. MATEC Web. Conf. **39**, 01001 (2016). https://doi.org/10.1051/matecconf/20163901001
34. M. Ahamed, M.J. Akhtar, M.A.M. Khan, Z.M. Alaizeri, H. Alhadlaq, Facile synthesis of Zn-doped Bi2O3 nanoparticles and their selective cytotoxicity toward cancer cells. ACS Omega **6**(27), 17353–17361 (2021a). https://doi.org/10.1021/acsomega.1c01467
35. M. Ahamed, M.J. Akhtar, M.M. Khan, H.A. Alhadlaq, SnO2-doped ZnO/reduced graphene oxide nanocomposites: synthesis, characterization, and improved anticancer activity via oxidative stress pathway. Int. J. Nanomed. **16**, 89–104 (2021b). https://doi.org/10.2147/ijn.s285392
36. K.A. Elsayed, M. Alomari, Q.A. Drmosh, A.A. Manda, S.A. Haladu, I. OlanrewajuAlade, Anticancer activity of TiO2/Au nanocomposite prepared by laser ablation technique on breast and cervical cancers. Opt. Laser Technol. **149**, 107828 (2022). https://doi.org/10.1016/j.optlastec.2021.107828
37. K. Kavithaa, M. Paulpandi, T. Ponraj, K. Murugan, S. Sumathi, Induction of intrinsic apoptotic pathway in human breast cancer (MCF-7) cells through facile biosynthesized zinc oxide nanorods. Karbala Int. J. Modern Sci. **2**(1), 46–55 (2016). https://doi.org/10.1016/j.kijoms.2016.01.002
38. X. Jiang, W. He, X. Zhang, Y. Wu, Q. Zhang, G. Cao, H. Zhang, J. Zheng, T.R. Croley, J.-J. Yin, Light-induced assembly of metal nanoparticles on ZnO enhances the generation of charge carriers, reactive oxygen species, and antibacterial activity. J. Phys. Chem. C. **122**(51), 29414–29425 (2018). https://doi.org/10.1021/acs.jpcc.8b10578
39. K.T. Nguyen, D.X.N. Mai, U.T.T. Doan, T.T. Nguyen, Y.T. Dang, H.K.T. Ta, T.B. Phan, N.K. Pham, The chitosan/ZnO bio-nanocomposites with selective antibacterial efficiency. J. Mater. Res. **36**(2), 508–517 (2021). https://doi.org/10.1557/s43578-020-00011-6